Available online at www.sciencedirect.com
ScienceDirect
Journal of the European Ceramic Society 27 (2007) 2355–2359
www.elsevier.com/locate/jeurceramsoc

Mesopores in nonstoichiometric oxides via oxyexsolution and Kirkendall effects

Ming-Yen Li [a], Pouyan Shen [a,*], Shyh-Lung Hwang [b]

[a] *Institute of Materials Science and Engineering, National Sun Yat-sen University, Kaohsiung, Taiwan, ROC*
[b] *Department of Materials Science and Engineering, National Dong Hwa University, Hualien, Taiwan, ROC*

Received 14 July 2006; received in revised form 2 October 2006; accepted 16 October 2006
Available online 28 November 2006

Abstract

Mesopores in nickel–cobalt oxide were synthesized through oxyexsolution at relatively low temperature for a controlled Kirkendall effect. A rapid net vacancy flux and a tensile misfit stress perpendicular to the protoxide/spinel interface caused the formation of elongated and aligned {1 0 0}-faceted mesopores in the spinel precipitates with a relatively low equilibrium vacancy concentration. Aligned mesopores in diffusion zone of nonstoichiometric metal oxides have potential applications on thermal barrier bond coating and mass-transport limited heterogeneous catalysis.

Keywords: Electron microscopy; Defects; Porosity; Diffusion; NiO/CoO

1. Introduction

Biomimetic assembly of inorganic-encased liquid crystals under the influence of amphiphilic template was widely used to fabricate mesoporous materials, following the pioneer work of Kresge et al.[1] In the solid state, however, pores form because of the difference in diffusion rates between two components in a diffusion couple as originally proved for metal alloys[2] and later binary oxide solid solution.[3,4] The Kirkendall pores thus formed in the CoO–NiO diffusion couple above 1000 °C were typically several micrometers in size.[3] Here, elongate mesopore variants were tailored in the spinel precipitates through an oxyexsolution process along a specific diffusion path in the NiO–CoO–O ternary. Instead of conventional diffusion couples, we employed a homogenization/sintering and then decomposition route for a more effective interdiffusion/oxyexsolution at the scale of individual grains with emphasis on the controlled nucleation and growth of mesopores in the spinel precipitate.

2. Experimental procedure

Experimentally, $Ni_{1-x}O$ and $Co_{1-x}O$ powders (Cerac, 325 mesh) in 1:2 molar ratio were ball milled in alcohol, oven dried at 100 °C, and then dry pressed at 650 MPa to form pellets ca. 5 mm in diameter and 2 mm in thickness. The pellets were homogenized/sintered at 1000 °C for 10 h in an open-air furnace and then quenched in air. Subsequent oxyexsolution was conducted at 720 °C for up to 72 h followed by cooling in the furnace. The experiment was therefore inter-diffusion between $Ni_{1-x}O$ and $Co_{1-x}O$ powders to form a homogeneous protoxide solid solution at 1000 °C, followed by annealing/oxidation at 720 °C in air to exsolve the spinel phase as in our previous study of oxidation-decomposition facilitated reorientation of nanoparticles in reactively sintered $(Ni_{0.33}Co_{0.67})_{1-\delta}O$ polycrystals.[5] The spinel was progressively Co-richer whereas the protoxide matrix progressively Ni-richer via a solid state diffusion path in the NiO–CoO–O ternary at 720 °C.[5] In this connection, $Co_{1-x}O$ was known to oxidize more rapidly to form Co_3O_4 spinel upon cooling below ca. 900–950 °C in air.[6]

X-ray diffraction (XRD, Cu Kα, 40 kV, 20 mA, at 0.05° and 3 s per step up to 2θ angle, 100°) was used to identify the phases in the heat-treated samples. The *d*-spacings measured from XRD trace were used for least-squares refinement of the lattice parameters.[7] The error of the *d*-spacing measurements on XRD trace and the refined lattice parameters were estimated to be ±0.0001 nm for homogenized sample and ±0.0002 nm for decomposed samples. Thin sections of the samples were Ar-ion milled to electron transparency for analytical electron micro-

* Corresponding author. Tel.: +886 7 5252000 4060; fax: +886 7 5254099.
E-mail address: pshen@mail.nsysu.edu.tw (P. Shen).

0955-2219/$ – see front matter © 2006 Elsevier Ltd. All rights reserved.
doi:10.1016/j.jeurceramsoc.2006.10.008

scopic (AEM, JEOL 3010) observations of the microstructures coupled with energy dispersive X-ray (EDX) analysis at 300 kV. The EDX analysis was performed using K shell counts for Co, Ni and O, and the principle of ratio method without absorption correction.[8]

3. Results

3.1. XRD

XRD indicated the sample heat-treated at 1000 °C for 10 h consists of rock salt-type protoxide with a fixed room temperature lattice parameter of 0.4233 ± 0.0001 nm, although minor amount of the spinel phase due to protoxide oxidation upon cooling in air was revealed by AEM. After further annealing at 720 °C for 2, 20 and 72 h, the protoxide solid solution has a progressively smaller lattice parameter of 0.4220 ± 0.0002, 0.4212 ± 0.0002 and 0.4206 ± 0.0002 nm, respectively. A smaller cell volume is due to the substitution of Ni^{2+} (effective ionic radii, 0.0690 nm) with Co^{2+} (0.0745 nm, high spin) in coordination number (C.N.) of 6.[9] The corresponding spinel upon annealing at 720 °C for 2, 20 and 72 h, has a decreasing lattice parameter of 0.8091 ± 0.0002, 0.8089 ± 0.0002 and 0.8084 ± 0.0002 nm, respectively. This was a result of Ni^{2+} expulsion to form double negatively charged nickel vacancies with concurrent oxidation of Co^{2+} to form smaller-size Co^{3+} (0.0545 nm) in the spinel structure. (The creation of a double negatively charged nickel vacancy in spinel was most likely charge balanced by two electron holes, i.e. losing two electrons from $2Co^{2+}$ to form $2Co^{3+}$.)

3.2. AEM

Transmission electron microscopic (TEM) and selected area electron diffraction (SAED) observations of the sample heat-treated at 1000 °C for 10 h showed minor spinel phase, which was overlooked by XRD. The spinel was precipitated in parallel epitaxial orientation from the protoxide (Fig. 1a) apparently during cooling from 1000 °C. These slab-like spinel precipitates were nucleated at dislocations and full of (1 0 0)-faceted elongate mesopores as viewed in the [0 1 1] zone axis. The elongate mesopores were aligned in the direction almost perpendicular to the spinel/protoxide interface and were more than one-order-of magnitude smaller in size than the inter- or intra-granular pores survived the sintering process.

Upon annealing at 720 °C for 2 h, the spinel precipitates and the mesopores within the spinel were both larger in number and size. The mesopores were basically extended along the direction perpendicular to the spinel/protoxide interfaces, i.e. {1 0 0} and {1 1 1} as viewed edge on in [0 1 1] zone axis (Fig. 1b). After further annealing at 720 °C for a total of 72 h, the spinel precipitates were coalesced into irregular/eqaunt shape (Fig. 1c). Meanwhile, the mesopores became smaller in number yet larger in size forming {1 0 0}-faceted variants, which were more or less coalesced as viewed with {1 0 0} faces edge on in [1 0 0] zone axis (Fig. 1c).

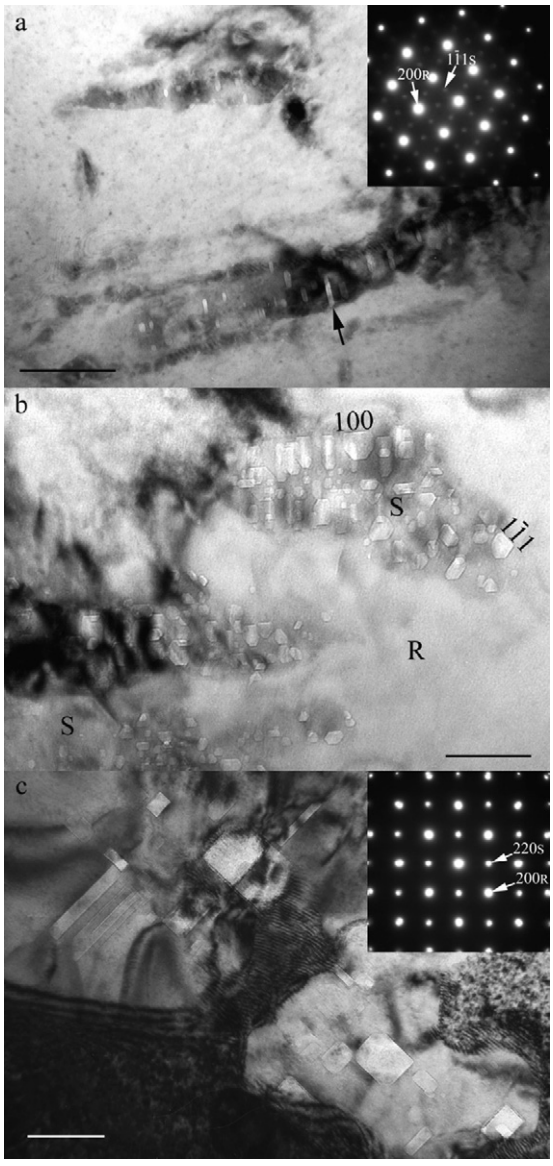

Fig. 1. Transmission electron micrographs (bright-field images) and selected area electron diffraction (SAED) patterns for mesoporous spinel precipitates (denoted as S) formed in various oxyexsolution stages from the homogenized $(Ni_{0.33}Co_{0.67})_{1-\delta}O$ protoxide with rock salt structure (denoted as R). (a) Slab-like spinel ([0 1 1] zone axis) with aligned elongate mesopores (arrow) formed during cooling from 1000 °C in air. (b) {1 0 0} and {1 1 1}-faceted spinel with such faceted mesopores in the sample annealed at 720 °C for 2 h. (c) Coarsened/coalesced spinel ([0 0 1] zone axis) with variants of {1 0 0}-faceted mesopores in the sample annealed at 720 °C for 72 h. Scale bars = 100 nm.

4. Discussion

The predominant formation of mesopores in the spinel phase relies on the equilibrium vacancy concentration of the spinel, a specific diffusion path in the NiO–CoO–O ternary, and the lattice mismatch between the co-existing protoxide and spinel, as addressed in turn.

4.1. Equilibrium vacancy concentration

The rate at which vacancies accumulate in a unit volume of the diffusion zone is given by[10]

$$\frac{dn_v}{dt} = -\text{div}\, J_v - \left[\frac{(n_v^{(e)}R)}{\tau}\right] \quad (1)$$

where n_v is the actual number of vacancies/unit volume, $n_v^{(e)}$ the equilibrium number, $R = n_v/n_v^{(e)} - 1$ the relative excess concentration, J_v the vacancy flux and τ is the vacancy lifetime. Assuming a vacancy lifetime of ~10 s for the Co-rich side at 1300 °C, the critical excess vacancy concentration (R_c) to form Kirkendall pores in the NiO–CoO diffusion zone was estimated to be 3.6×10^{-2}.[4] A longer τ at lower temperature would require a larger R_c to condense vacancies unless the lattice was transformed into $Co_{3-\delta}O_4$ spinel with a lower $n_v^{(e)}$, i.e. less extent of nonstoichiometry ($\delta = 0.0002$[11]) than $Co_{1-x}O$ ($x = 0.01$[12]) and $Ni_{1-x}O$ ($x = 0.001$[13]). A lower equilibrium vacancy concentration would then favor the condensation of pores in the spinel structure. It should be noted that the defect clusters in the spinel[11] might act as nucleation sites for many mesopores. By contrast, within a much smaller volume of cobalt nanocrystal upon oxidation/sulfidation in colloidal solution, the supersaturated vacancy cloud was coalesced into a single void.[14] (Hollow nanocrystals were synthesized by oxidation/sulfidation of cobalt colloidal solution with an additional mechanism analogous to the Kirkendall effect, in which pores form because of the difference in diffusion rates between two components in a diffusion couple.[14])

4.2. Diffusion path

The vacancy flux in Eq. (1) was affected by the precipitation of the spinel phase along a specific path in the NiO–CoO–O ternary either upon cooling from 1000 °C or dwelling at 720 °C in air. The XRD results indicated that the homogenized $(Ni_{0.33}Co_{0.67})_{1-\delta}O$ protoxide was rapidly oxidized as spinel, which became progressively Co-richer at the expense of the protoxide progressively Ni-richer as the dwelling time increases at 720 °C.[5] Outward diffusion of Ni and inward diffusion of Co for the spinel was also indicated by point-count EDX profile across the slab-like spinel in a representative sample fired at 720 °C for 2 h.[5] Based on the composition dependence of lattice parameters for the spinel $Ni_xCo_{3-x}O_4$,[15] the diffusion path of the present samples annealed at 720 °C for 2–72 h in air was constructed (Fig. 2). The final composition of the protoxide and the spinel in the sample annealed at 720 °C for 72 h turned out to be $(Ni_{0.65}Co_{0.35})_{1-\delta}O$ and $(Ni_{0.05}Co_{0.95})_3O_4$, respectively, in accordance with the tie line.[16] Assuming local equilibrium in a diffusion-controlled process, a narrow spinel slab in the nascent precipitation stage (i.e. upon cooling from 1000 °C or onset annealing at 720 °C in air) would have a steep Ni concentration gradient (Fig. 3). In other words, there was rather effective inward flux of nickel vacancies for an explosive nucleation of pores in the initial transient, as manifested by the rapid formation of the mesoporous spinel upon quenching from 1000 °C in air (Fig. 1a). It should not be excluded that the flux of double positively charged oxygen vacancies in the diffusion path of the NiO–CoO–O ternary (Fig. 2) helps condense the pores at 720 °C. In any case, the vacancy condensation process could be effective at positions with high vacancy creation rate, as constrained by the derivative of the net vacancy flux.[17] The pores generated in the spinel could coalesce by Brownian motion of the bubbles, which involves atoms movement from its leading surface to the trailing surface via surface diffusion rather than evaporation.[18] The stress, in the vicinity of a dislocation or near the interphase interface with a considerable lattice mismatch as addressed in the next section, is also of concern to the formation of mesopores.

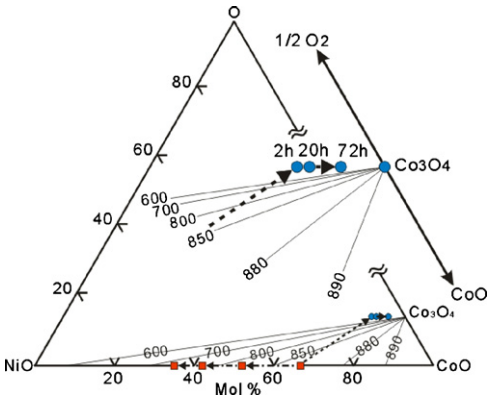

Fig. 2. NiO–CoO–O isothermal section at 720 °C showing the diffusion path upon aging with accompanied oxidation/precipitation to form the $(Ni_{0.05}Co_{0.95})_3O_4$ spinel as depicted in a further magnified view inset. Note tie lines at specified temperatures in celsius.[16] Red square and blue circle denote protoxide and spinel, respectively. (For interpretation of the references to color in this figure legend, the reader is referred to the web version of the article.)

4.3. Lattice mismatch

Uneven mass fluxes in a binary diffusion couple are known to create a tensile stress state in the region suffering a loss of

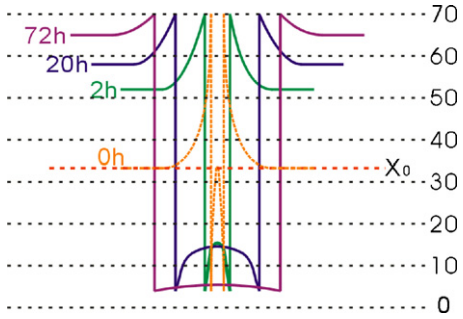

Fig. 3. Schematic drawing of unidirectional concentration gradient of Ni in atomic percent of cations across the slab-like spinel precipitate progressively widened from 2 to 72 h at 720 °C, assuming local equilibrium at the interface. The starting composition of protoxide was denoted as X_0 (red dashed line) and the initial transient for the case of oxyexsolution upon cooling from 1000 °C to 720 °C was depicted as orange dotted curve ($t = 0$ h) exaggerated for clarity. The transient compositions of the spinel and protoxide are based on XRD lattice parameters. Note the Ni gradient in both protoxide and spinel became less steep following a nearly constant O/(Ni + Co) path in the NiO–CoO–O ternary of Fig. 2. (For interpretation of the references to color in this figure legend, the reader is referred to the web version of the article.)

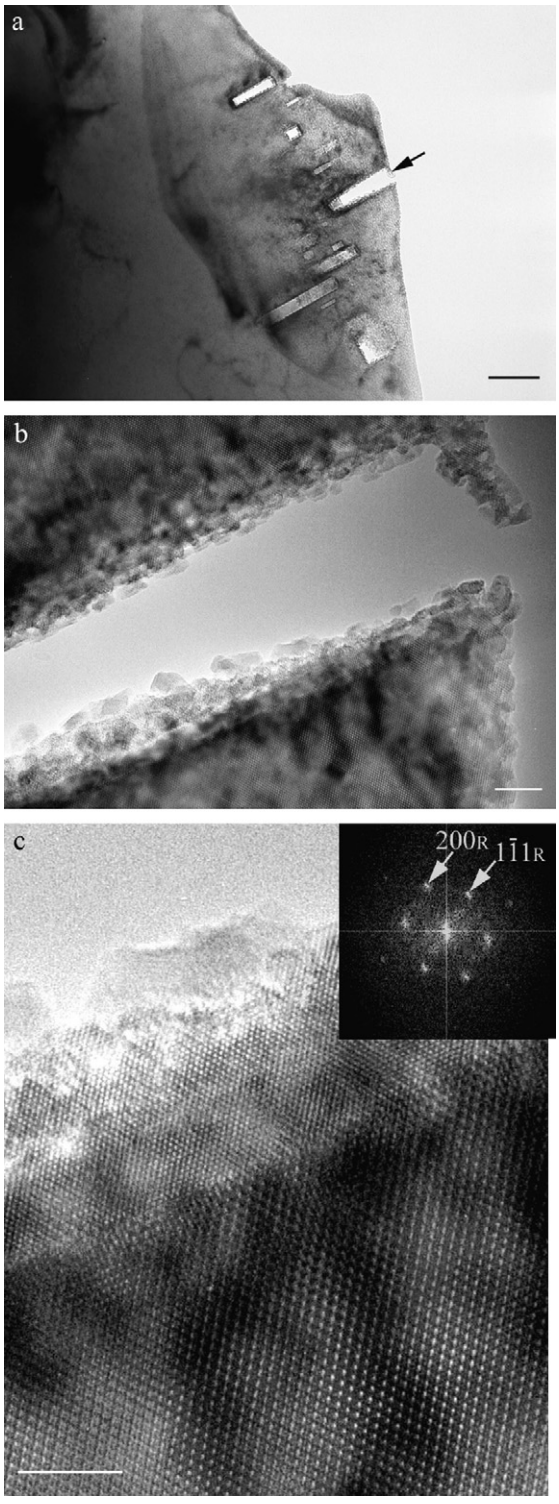

Fig. 4. (a) Transmission electron micrograph (bright-field image) of the mesopores in the spinel precipitates with $Co_{1-x}O$-decorated rim formed upon annealing at 720 °C for 72 h in air. (b) Lattice image from the Ar-thinned area (arrow) in (a). (c) Further magnified view with inset Fourier transform ([0 1 1] zone axis) showing that the $Co_{1-x}O$ rim of rock salt structure (denoted as R) and the spinel (denoted as S) have parallel epitaxial relationship. Scale bars, $a = 100$ nm, $b = 10$ nm and $c = 5$ nm.

mass, causing the formation of Kirkendall pores in the region.[17] The condensation of vacancies in the spinel rather than protoxide can also be rationalized by a tensile stress on the spinel side. This argument is justified by the net mass loss of ~1/4 cations, i.e. change from 4(Ni, Co)O to $\sim Co_3O_4$, and resulting smaller half-cell volume of the spinel ($0.5V_S$) than the cell volume of the rock salt-type protoxide (V_R). In fact, there was a considerable tensile stress for the spinel throughout its oxyexsolution from the protoxide, as indicated by the volume mismatch $(V_R - 0.5V_S)/V_R = 0.119$, 0.115 and 0.112 upon annealing at 720 °C for 2, 20 and 72 h, respectively assuming a negligible thermal expansion effect on the cell volume.

In the nascent oxyexsolution stage, there was unidirectional tensile stress perpendicular to the well-developed spinel/protoxide interface. Therefore the elongate mesopores tended to be aligned in a single direction within the slab-like spinel. In the later stage, however, the elongate mesopores formed variants in the coarsened/coalesced spinel precipitates probably because of the increased dimensionality of net vacancy flux and more complicated stress state.

It should be noted that the spinel approached the $Co_{3-\delta}O_4$ composition when the sample was annealed at 720 °C for 72 h (Fig. 2). Under such a circumstance, the confined mesopores in the spinel were decorated with newly formed $Co_{1-x}O$ protoxide (Fig. 4a). Lattice image and 2-D Fourier transform (Fig. 4b and c) indicated that such a new protoxide frame is in parallel epitaxial relationship with the spinel and has a $d_{(1\,1\,1)}$-spacing of 0.2458 nm in accord with $Co_{1-x}O$ (0.2460 nm, JCPDS file 09-0402) rather than $Ni_{1-x}O$ (0.2410 nm, JCPDS file 04-0835). We suggest that relatively low oxygen partial pressure in the confined pores would cause reduction of the $Co_{3-\delta}O_4$ spinel and/or a sublimation/condensation process to form $Co_{1-x}O$ at the pore surface. By contrast, the interconnected mesopores with possible access to open air in the same sample (cf. some in Fig. 1c) are immune from such a $Co_{1-x}O$ frame.

5. Conclusions

In essence, elongate mesopores in nonstoichiometric transition metal oxides can be tailored via oxyexsolution/Kirkendall effects under the influence of lattice misfit stress. Unidirectional pore formation may have commercial importance in the production of aligned microstructure with low weight for prostheses/catalyst supports[19] involving mass-transport limited heterogeneous process.[20] In particular, the aligned elongate mesopores in nickel–cobalt spinel oxide have potential applications to electrocatalysis in anodic processes. A mesoporous nickel–cobalt spinel oxide as the thermal barrier bond coating on Ni/Co-based super alloys is expected to have a beneficial high strain tolerance, spallation resistance and lower thermal conductivity.[21]

Acknowledgements

We thank Steven Chen for helpful discussions and an anonymous referee for constructive comments. Supported by the Center for Nanoscience and Nanotechnology of NSYSU and

National Science Council, Taiwan under contract NSC 92-2216-E-110-005.

References

1. Kresge, C. T., Leonowicz, M. E., Roth, W. J., Vartuli, J. C. and Beck, J. S., Ordered mesoporous molecular sieves synthesized by a liquid-crystal template mechanism. *Nature*, 1992, **359**, 710–712.
2. Smigelskas, A. D. and Kirkendall, E. O., Zinc diffusion in alpha brass. *Trans. Met. Soc. AIME*, 1947, **171**, 130–142.
3. Stiglich, J. J., Interdiffusion and defect structure in NiO–CoO solid solution. Ph.D. thesis, Northwestern University, Evanston, IL, 1970.
4. Stiglich, J. J., Cohen, J. B. and Whitmore, D. H., Interdiffusion in CoO–NiO solid solutions. *J. Am. Ceram. Soc.*, 1973, **56**(3), 119–126.
5. Li, M. Y., Shen, P. and Hwang, S. L., Oxidation-decomposition facilitated reorientation of nanoparticles in reactively sintered $(Ni_{0.33}Co_{0.67})_{1-\delta}O$ polycrystals. *Mater. Sci. Eng. A*, 2003, **343**, 227–234.
6. Oku, M. and Sato, Y., In situ X-ray photoelectron spectroscopic study of the reversible phase transition between CoO and Co_3O_4 in oxygen of 10^{-3} Pa. *Appl. Surf. Sci.*, 1992, **55**, 37–41.
7. Holland, T. J. B. and Redfern, S. A. T., Unit cell refinement from powder diffraction data: the use of regression diagnostics. *Mineralogical Magazine*, 1997, **61**, 65–77.
8. Williams, D. B., *Practical Analytical Electron Microscopy in Materials Science*. Philips Electronic Instruments, Mahwah, 1984, pp. 64–74.
9. Shannon, R. D., Revised effective ionic radii and systematic studies of interatomic distances in halides and chalcogenides. *Acta Cryst. A*, 1976, **32**, 751–767.
10. Seitz, F., On the porosity observed in the Kirkendall effect. *Acta Metall.*, 1953, **1**, 355–369.
11. Lee, W. H. and Shen, P., $Co_{3-\delta}O_4$ paracrystal: 3-D assembly of nanosize defect clusters in spinel lattice. *J. Solid State Chem.*, 2004, **177**, 101–108.
12. Tomlinson, S. M., Catlow, C. R. A. and Harding, J. H., Computer modeling of the defect structure of non-stoichiometric binary transition metal oxides. *J. Phys. Chem. Solids*, 1990, **51**, 477–506.
13. Sockel, H. G. and Schmalzried, H., Coulometric titration in transition metal oxides. *Ber. Bunsenges. Phys. Chem.*, 1968, **72**(7), 745–754.
14. Yin, Y., Rioux, R. M., Erdonmez, C. K., Hughes, S., Somorjai, G. A. and Alivisatos, A. P., Formation of hollow nanocrystals through the nanoscale Kirkendall effect. *Science*, 2004, **304**, 711–714.
15. Ríos, E., Nguyen-Cong, H., Marco, J. F., Ganvedo, J. R., Chartier, P. and Gautier, J. L., Indirect oxidation of ethylene glycol by peroxide ion at $Ni_{0.3}Co_{2.7}O_4$ spinel oxide thin film electrodes. *Electrochimica. Acta*, 2000, **45**, 4431–4440.
16. Moore, R. J. and White, J., Equilibrium relationships in the system NiO–CoO–O_2. *J. Mater. Sci.*, 1974, **9**, 1393–1400.
17. Porter, D. A. and Easterling, K. E., *Phase Transformations in Metals and Alloys*. Chapman & Hall, London, 1992, pp. 1–446.
18. Barnes, R. S. and Mazey, D. J., The migration and coalescence of inert gas bubbles in metals. *Proc. Roy. Soc.*, 1963, **275**, 47–57.
19. Padture, N. P., Schlichting, K. W., Bhatia, T., Ozturk, A., Cetegen, B., Jordan, E. H. *et al.*, Towards durable thermal barrier coatings with novel microstructures deposited by solution-precursor plasma spray. *Acta Mater.*, 2001, **49**, 2251–2257.
20. Bond, G. C., *Heterogeneous Catalysis: Principles and Applications*. Oxford University Press, Oxford, 1987, pp. 1–176.
21. Padture, N. P., Gell, M. and Jordan, E. H., Thermal barrier coatings for gas-turbine engine applications. *Science*, 2002, **296**, 280–284.